

Article

# Optimally Initialized Model Reference Adaptive Controller of Wearable Lower Limb Rehabilitation Exoskeleton

Mohammad Soleimani Amiri <sup>1</sup>, Rizauddin Ramli <sup>1,\*</sup> and Ahmad Barari <sup>2</sup>

<sup>1</sup> Department of Mechanical and Manufacturing Engineering, Faculty of Engineering and Built Environment, Universiti Kebangsaan Malaysia, Bangi 43600, Selangor, Malaysia

<sup>2</sup> Advanced Digital Design, Manufacturing, and Metrology Laboratories (AD2MLabs), Department of Mechanical and Manufacturing Engineering, Faculty of Engineering and Applied Science, Ontario Tech University, Oshawa, ON L1G 0C5, Canada

\* Correspondence: rizauddin@ukm.edu.my

**Abstract:** A wearable lower-limb rehabilitation exoskeleton functions to fulfill the recovery process of limb functionality and assist physiotherapists. This paper presents an optimized adaptive control system for a wearable lower-limb rehabilitation exoskeleton. The tuning of the controller gains is defined as an optimization problem for a closed-loop control system of the wearable lower-limb rehabilitation robot by genetic algorithm and particle swarm optimization. We presented a novel initialized model reference adaptive controller (IMRAC) for real-time joint trajectory tracking, in which controller gains are adjusted by the gradient-based method. An experimental test of a 4-degree of freedom lower-limb rehabilitation exoskeleton was carried out to observe the closed-loop performance of IMRAC for bipedal human walking. The statistical comparison between IMRAC and MRAC shows an efficient performance and robustness of our proposed method for the joint trajectory tracking of the lower-limb rehabilitation exoskeleton in real time.

**Keywords:** model reference adaptive controller; exoskeleton; genetic algorithm

**MSC:** 93A99; 49N25



**Citation:** Amiri, M.S.; Ramli, R.; Barari, A. Optimally Initialized Model Reference Adaptive Controller of Wearable Lower Limb Rehabilitation Exoskeleton. *Mathematics* **2023**, *11*, 1564. <https://doi.org/10.3390/math11071564>

Academic Editors: Honglei Xu and Lingyun Wang

Received: 24 February 2023

Revised: 16 March 2023

Accepted: 17 March 2023

Published: 23 March 2023



**Copyright:** © 2023 by the authors. Licensee MDPI, Basel, Switzerland. This article is an open access article distributed under the terms and conditions of the Creative Commons Attribution (CC BY) license (<https://creativecommons.org/licenses/by/4.0/>).

## 1. Introduction

One of the main reasons for walking disabilities is neurological impairments caused by spinal cord injuries and stroke [1,2]. Satisfactory rehabilitation training is essential to minimize the negative consequences of chronic health conditions [3]. These impairments affect the daily life of disabled people, which requires physiotherapists to use rehabilitation support devices for recovering paralyzed patients. The use of a lower-limb rehabilitation robot or exoskeleton has been popular, as a wearable apparatus to aid patients who suffer from mobility problems [4].

The wearable lower-limb rehabilitation robot is principally organized for subjects with muscle injuries and mobility disabilities to improve their motor ability in daily activities. In the initial stages of rehabilitation, the patient's joints are mostly in a passive condition. Therefore, the wearable lower-limb rehabilitation robot supports and guides the joint to its desired trajectory, and patients are keen to perform exercises with minimized muscle activity and metabolism [5–7].

The desired trajectories of limb joints are difficult to follow smoothly with lower a steady-state error and robust performance due to disturbances and uncertainties [8,9]. To conquer this issue, a robust control system is needed to reduce a steady-state error and provide stability in the presence of disturbance. Huo et al. [10] proposed an active impedance control strategy for sit-to-stand conditions. They carried out an experiment with a healthy human subject to measure the effectiveness-proposed controller. They proved that their control system bounded the tracking error within a limited range. Lin et al. [11]

designed the desired closed-loop Hamiltonian system and the corresponding control law for the hip–knee exoskeleton. They validated their method on walking and sit-to-stand situations to demonstrate the versatility of this control approach and its effect on muscular effort.

In the other study, Lu et al. [12] used an adaptive control system to overcome disturbances and unknown parameters by the Lyapunov approach. Tu et al. [13] studied a sliding mode adaptive control strategy for a four degrees-of-freedom (DoF) lower-limb rehabilitation robot. They presented two outer loops with a parameter admittance controller for estimating the active muscle strength and an inner loop for adaptive sliding mode control strategy. Huang et al. [14] presented a mathematical model for gait trajectory and a control strategy based on the hybrid of fuzzy logic control and the Lyapunov approach. They integrated a disturbance observer into their proposed adaptive controller design to compensate for the uncertain disturbance to obtain an effective tracking performance. They designed experiments on two healthy subjects on a walking exoskeleton. The results showed that their proposed method can be applied to walking exoskeletons to enhance human mobility.

The precision of the controller parameters tuning is one of the challenges in establishing a control system. This issue has been attracting significant interest among researchers. Shan et al. [15] applied a proportional–integral–derivative (PID) and a fuzzy controller for a wearable 1 DoF orthosis with an active knee joint for walking assistance to reduce the consumption of muscular power by the wearer during gait training. Belkadi et al. [16] modified particle swarm optimization (PSO) with random initial gains of the PID controller for minimizing the trajectory error of the lower-limb rehabilitation exoskeleton. They validated their proposed controller in the simulation of a wearable lower-limb rehabilitation robot and compared the PID controller tuned by PSO with constant parameters. They proved that their tuning method performed better by using numerical analysis. Zhang et al. [17] classified the control part of the lower-limb rehabilitation robot into stand and swing phases. They analyzed the kinetic model for both phases and employed the sliding mode and fuzzy compensation method to reduce the disturbances in the swing phase. Meanwhile, the cerebellar model articulation and PID controller for stance and swing phases have been established for stabilizing the control system. Yang et al. [18] studied a robust learning controller based on the Lyapunov approach to control an exoskeleton robot with hybrid electro-hydraulic actuators, and they validated the learning control method in the presence of a periodic reference. Due to the reliable stability of adaptive control system and precision of the optimization methods, in this paper, an optimal adaptive control method is used to improve tracking trajectory controller.

From the literature [10–18], several control strategies have been developed to improve the tracking effectiveness of nonlinear systems. The aim of using an adaptive control strategy is to increase the robustness and stability of the nonlinear dynamic system. This work develops an optimally adaptive control scheme for the walking cycle of an exoskeleton robot. The contribution of this paper is as follows:

- This work compares the optimal tuning of controller parameters by two different optimization methods, i.e., genetic algorithm (GA) and PSO for the mathematical model of an exoskeleton.
- It proposes an initialized model reference adaptive controller (IMRAC) for a walking cycle of the lower-limb exoskeleton robot to obtain an efficient tracking performance.
- It explains that the proposed control scheme is initialized by the optimized tuned parameters to improve its efficiency.

The contents of this paper are as follows: Section 2 represents the structure of the wearable lower-limb rehabilitation robot and its mathematical model. Section 3 addresses the closed-loop control and optimal tuning of controller gains. In Section 4, the formulation for IMRAC is presented. Section 5 covers the stability analysis of the control strategy. In Section 6, the efficiency of the IMRAC control system is verified by the experiment. Section 7 concludes this paper.

## 2. Overview of Wearable Lower-Limb Exoskeleton

### 2.1. Exoskeleton Design

Since the aim of the lower-limb exoskeleton is to be used by patients with muscle injuries to enhance mobility in daily activities, we developed a walking exoskeleton with 4 DoFs. The wearable lower-limb rehabilitation exoskeleton prototype consists of two active joints for the hip and knee. The joints of the exoskeleton are flexion and extension joints and rotate in pitch directions. The control package consisting of the batteries, motor drivers, microprocessor, and an on-board computer is located at the back of the exoskeleton. Figure 1 represents the structure of the wearable lower-limb exoskeleton.



Figure 1. Structure of the wearable lower-limb exoskeleton.

The lengths of the thigh and shank links are fixed, with heights of 42 cm and 40 cm, respectively. Table 1 exhibits detailed information of the wearable lower-limb rehabilitation robot.

Table 1. Motion and DoFs of the wearable lower-limb rehabilitation robot.

DoFs	Motion	Property
Left hip and right hip	Flexion and extension	Active
Left knee and right knee	Flexion and extension	Active

### 2.2. Hardware Structure

Hip and knee joints are actuated by brushed DC motors with the 9.6 Nm nominal torque. The motor drivers are used for DC motors to provide precise voltages by adjusting the duty of pulse width modulation. In order to sense the feedback signals, a quadrature optical encoder is attached to the actuator’s shaft. An 8-bit board microprocessor, which is programmed by C++, is used to control and regulate the input voltage and direction of the motors. The control system is programmed in Python and runs on a PC with an Intel Core i3 CPU and 16 GB RAM. In addition, the exoskeleton is equipped with Raspberry Pi 4 with 8 GB RAM as the onboard processor, rotary encoder, and force sensors. The microprocessor, motor driver, and encoders are connected to the onboard processor. The acquitted data are transferred by WiFi to the PC to run the control strategy and human interaction interface for the physiotherapist and patient.

### 2.3. Dynamic Model

Dynamic of the lower-limb exoskeleton is modeled by Newton–Euler principle as follows,

$$M(\theta)\ddot{\theta} + C(\theta, \dot{\theta}) + G(\theta) = u \tag{1}$$

where  $M(\theta) \in \mathbb{R}^{n \times n}$  represents the inertia matrix,  $\theta \in \mathbb{R}^n$  is the joint angle,  $C(\theta, \dot{\theta}) \in \mathbb{R}^n$  is centripetal and Coriolis vector,  $G(\theta) \in \mathbb{R}^n$  introduces the gravitational force, and  $u \in \mathbb{R}^n$  is the control output. In this paper, the mathematical model is determined using system identification in our previous study by Amiri et al. [19]. The identified system estimated the unknown parameters of the mathematical model in Laplace form as follows

$$G_i(s) = \frac{\theta(s)}{u(s)} = \frac{b_i}{a_{1_i}s^3 + a_{2_i}s^2 + a_{3_i}s + a_{4_i}} \tag{2}$$

where  $G_i(s)$  represents the hip and knee mathematical models in frequency domain.  $b_i$  and  $a_{j_i}, j = 1, 2, 3, 4$  are the unknown parameters. Since the wearable lower-limb rehabilitation robot is symmetrical, we simplify it as only one leg manipulator for the control strategy. Table 2 illustrates the parameters of the mathematical model for each joint obtained by system identification in MATLAB.

**Table 2.** Parameters of mathematical model for each joint.

	$b_i$	$a_{1_i}$	$a_{2_i}$	$a_{3_i}$	$a_{4_i}$
Hip ( $i = 1$ )	26.4499	0.001	0.2362	1.606	4.6603
Knee ( $i = 2$ )	25.9909	0.001	0.0641	0.5658	1.7326

### 3. Optimal Controller Strategy

#### 3.1. Optimization Problem

The optimization is utilized to tune the angle of each wearable lower-limb rehabilitation robot joint with efficient performance for the repetitive tasks of the gait cycle. For each joint, a control system is established for angular trajectory tracking. The control law is represented as follows

$$u = KZ \tag{3}$$

where

$$Z = e + \Lambda \dot{e} \tag{4}$$

where  $K \in \mathbb{R}^{n \times n}$  and  $\Lambda \in \mathbb{R}^{n \times n}$  are the symmetrical diagonal matrices that contain controller gains and  $u$  is the controller output.  $e$  is the steady-state error given as follows

$$e = \theta_d - \theta \tag{5}$$

where  $\theta_d \in \mathbb{R}^{n \times 1}$  and  $\theta \in \mathbb{R}^{n \times 1}$  are the desired and actual angular trajectories. In the frequency domain, the controller law in Equation (3) is given as follows

$$C(s) = \frac{u(s)}{e(s)} = K(1 + \Lambda s) \tag{6}$$

where  $C(s)$  is the controller in the frequency domain. The objective function is determined while the input of the closed-loop control system is set as an unit step response [20]. Hence, steady-state error for the optimization problem  $e_{obj}(s)$  is represented as

$$e_{obj}(s) = 1 - \frac{C(s)G_i(s)}{1 + C(s)G_i(s)} \tag{7}$$

In this work, an objective function based on the integral time absolute error (ITAE) was used. ITAE is the integration of absolute error with time  $t$  weighted by elapsed time [21]. Then, we have

$$f_{obj} = \int_0^t t |e_{obj}(t)| dt \tag{8}$$

where  $t$  represents the elapsed time.  $e_{obj}(t)$  is the time domain steady-state error. Hip and knee joints are actuated by brushed DC motors with 9.6 Nm nominal torque. The motor drivers are used for DC motors to provide precise voltages by adjusting the duty of pulse width modulation. In order to sense the feedback signals, a quadrature optical encoder is attached to the actuator’s shaft. An 8-bit board microprocessor, programmed by C++, is used to control and regulate the input voltage and direction of motors. The control system is programmed in Python and runs on a PC with an Intel Core i3 CPU and 16 GB RAM. In addition, the exoskeleton is equipped with Raspberry Pi 4 with 8 GB RAM as the onboard processor, rotary encoder, and force sensors. The microprocessor, motor driver, and encoders are connected to the onboard processor. The acquitted data are transferred by WiFi to the PC to run the control strategy and human interaction interface for the physiotherapist and patient.

### 3.2. Controller Tuning by GA

GA is an iterative algorithm, in which the generations are developed by using crossover and mutation. One of the GA’s advantages is the low chance of being trapped on a local optimum [22]. The design variables of the GA are the gains of the controller.

By generating an initial population of random values, each gene is evaluated by the objective function. Then, genes are sorted based on the objective function evaluation in ascending order. The next generations are set up by crossover and mutation. Crossover extracts the genes from the populations and recombines them to enhance the chance of concluding minimal results. Mutation remains the diversity of GA from one generation to the next one.

During the evaluation process, 5% of the previous population remain unchanged as elite genes. The evaluation is a repetitive process after establishing each generation. Each gene carries the controller gains as follows,

$$x_{i,j} = [K \ \Lambda]_{ij} \tag{9}$$

where  $j$  and  $i$  express the number of population and iteration, respectively. The GA pseudocode is illustrated in Algorithm 1.

---

#### Algorithm 1 GA pseudocode

---

- 1: Start
  - 2: Random initialization for population with 40 genes;
  - 3: Evaluation;
  - 4: **while** Number of generation is not greater than 400 **do**;
  - 5:     Set up generations by crossover and mutation;
  - 6:     Apply objective function;
  - 7:     Sort in ascending order;
  - 8: **end while**
  - 9: End
- 

Figure 2 shows the objective function over the iteration for GA.

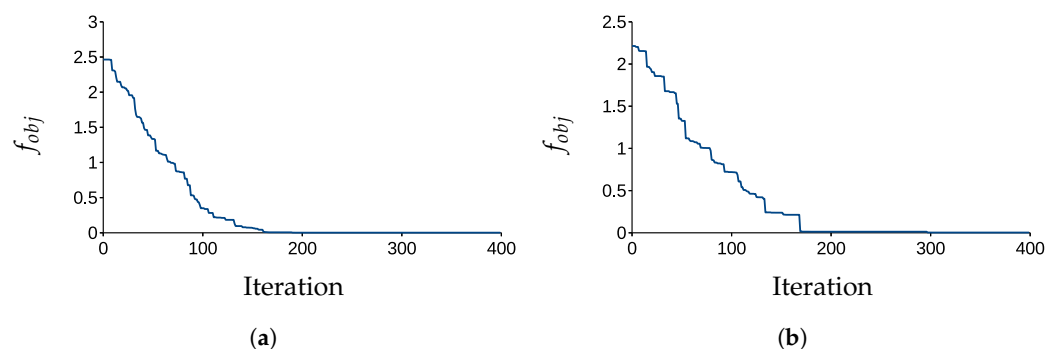


Figure 2.  $f_{obj}$  of GA in each iteration. (a) hip; and (b) knee.

As can be seen in Figure 2, GA needs 166 iterations to converge to zero. The final values of the hip and knee are  $9.7 \times 10^{-6}$  and  $1.1 \times 10^{-4}$ , respectively. Table 3 illustrates the tuned gains by GA.

**Table 3.** Optimized gains by GA.

	K	Λ
Hip	1.6017	2.1741
Knee	2.7663	8.9214

### 3.3. Controller Tuning by PSO

PSO is an iterative optimization method inspired by biological societies such as a flock of birds, school of fish, and a swarm of bees [23]. It is uncomplicated to implement in different optimization problems. The robustness of its parameters is controllable [24]. In addition, PSO has rapid convergence and there is a low possibility of being trapped in the neighboring set of candidate solutions [25]. The optimization parameters are changed by increasing the number of iterations to grow the chance of finding the global optimum. Equation (10) represents the next iteration’s particles, which are the summation of the position of previous particles with their velocity.

$$x_{i,j} = x_{i-1,j} + v_{i,j} \tag{10}$$

where  $j$  and  $i$  are the numbers of particle and iterations, respectively;  $x_{i-1,j}$  is the position of particles of the previous iteration, and  $v_{i,j}$  is the velocity and direction of the current particle toward the next iteration expressed as follows.

$$v_{i,j} = \omega_i v_{i-1,j} + C_1 \zeta_1 (p_{best,i-1} - x_{i,j}) - C_2 \zeta_2 (g_{best} - x_{i,j}) \tag{11}$$

where  $\zeta_1$  and  $\zeta_2$  are randomly established between 0 and 1.  $C_1$  and  $C_2$  are positive coefficients of the self-recognition component, and social components, respectively (Figure 3).

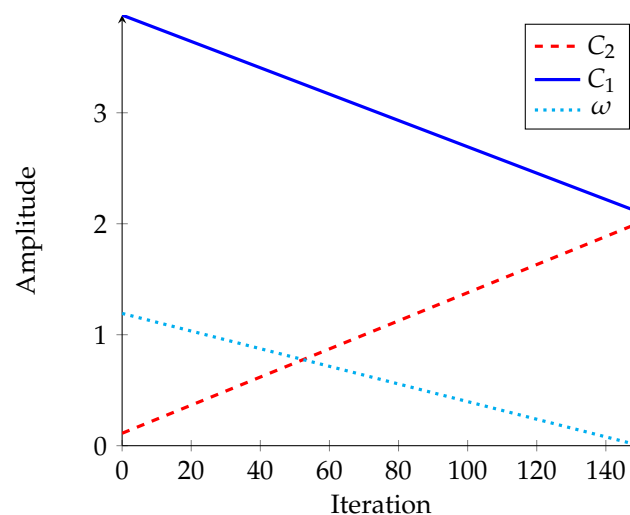


**Figure 3.** Changes in PSO parameters.

$p_{best,i}$  and  $g_{best}$  are the best position and the global best of each population, respectively.  $\omega_i$  denotes the inertia weight, where its value is readjusted per iteration, given as follows,

$$\omega_i = \omega_d \omega_{i-1} \tag{12}$$

where  $\omega_d$  is damping value. The objective function is determined for evaluation. Each particle of each iteration with the lowest objective function is selected as  $p_{best,i}$ . After evaluation,

the lowest  $p_{best,i}$  is defined as the global best  $g_{best}$ . Algorithm 2 exhibits the pseudocode of PSO.

**Algorithm 2** PSO pseudocode

- 1: Start;
- 2: Random initialization of the first population with 30 particles;
- 3: Evaluation and sorting;
- 4: Set the initial  $p_{best}$
- 5: **while** Number of iteration < 150 **do**;
- 6:     Generate new iteration;
- 7:     Obtain the  $p_{best}$ ;
- 8:     **if**  $p_{best} < g_{best}$  **then**;
- 9:         Set it as  $g_{best}$
- 10:    **end if**
- 11: **end while**
- 12: Select final  $g_{best}$  as the result;
- 13: End

Figure 4 represents the objective function of the PSO, which shows that it gradually converges towards zero with every iteration.

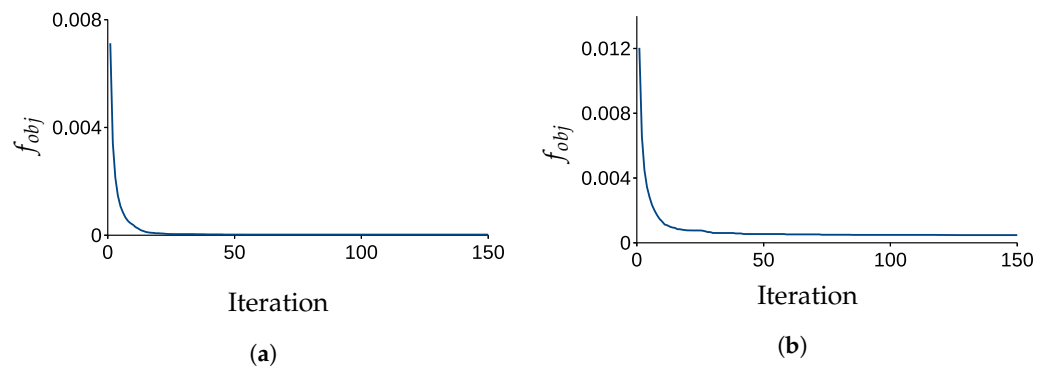


**Figure 4.**  $f_{obj}$  in each iteration for PSO. (a) Hip; and (b) Knee.

As can be seen in Figure 4, after 70 and 50 iterations, the objective function converges to zero for the hip and knee. The final values of the hip and knee are  $8.7 \times 10^{-8}$  and  $1.5 \times 10^{-5}$ , respectively. Table 4 demonstrates the optimal parameters of the controller gains tuned by PSO.

**Table 4.** Controller gains tuned by PSO.

	K	Λ
Hip	5.3422	19.9215
Knee	6.9391	22.4260

**4. IMRAC Strategy**

In this paper, IMRAC is determined to control the joint trajectory in real-time. The gains of the controller are obtained based on the simulated mathematical model of the wearable lower-limb rehabilitation exoskeleton. In addition, a model reference is designed to determine the ideal behavior of the control system [26,27]. The adaptive controller is fed by the difference between the model reference model and actual trajectory to adjust the controller parameters. Figure 5 shows a block diagram of the proposed optimal adaptive control strategy.

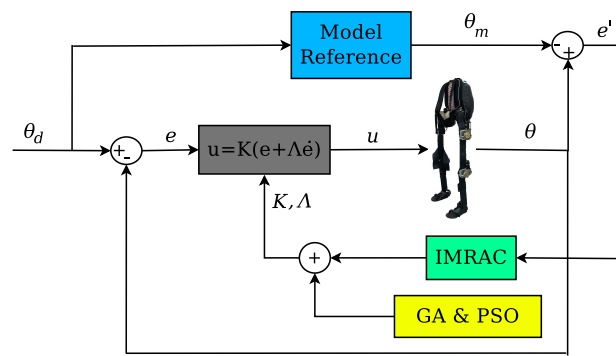


Figure 5. Block diagram of the IMRAC strategy.

$\theta_m$  and  $\dot{e}$  are the model reference angular trajectory and tracking error, which is the difference between the model reference  $\theta_m$  and the actual  $\theta_{act}$  trajectory.

$$\dot{e} = \theta_{act} - \theta_m \tag{13}$$

Thus, the fitness function of IMRAC is minimized as follows,

$$J(\beta) = \frac{1}{2} \dot{e}_m^2 \tag{14}$$

where  $\beta = [K \ \Lambda]^T$  is the controller gains matrix. The changes in  $\beta$  in the direction of the negative gradient of  $J$  is given by

$$\frac{d\beta}{dt} = -\sigma \frac{\partial J}{\partial \beta} = -\sigma \frac{\partial J}{\partial \dot{e}} \frac{\partial \dot{e}}{\partial \beta} \tag{15}$$

where the negative sign implies that  $\beta$  changes to minimize  $J$ ;  $\frac{\partial \dot{e}}{\partial \beta}$  is the sensitivity derivatives of the tracking error. The  $\sigma$  represents the speed of adaption. Therefore,

$$\frac{\partial J}{\partial \dot{e}} = \dot{e} \tag{16}$$

Thus, Equation (15) is rewritten as follows,

$$\frac{d\beta}{dt} = -\sigma \dot{e} \frac{\partial \dot{e}}{\partial \beta} \tag{17}$$

The exoskeleton model in the frequency domain is represented as follows,

$$\frac{\theta(s)}{u(s)} = HG(s) \tag{18}$$

where  $H$  is the unknown positive constant. The model reference is given as follows,

$$\frac{\theta_m(s)}{\theta_d(s)} = H_0 G(s) \tag{19}$$

where  $H_0$  is a positive constant. The sensitivity derivatives of the tracking error are given as follows,

$$\frac{\partial \dot{e}}{\partial \beta} = HG(s)\theta_d \tag{20}$$

Consequently, Equation (17) is reconsidered as follows,

$$\frac{d\beta}{dt} = -\sigma \dot{e} HG(s)\theta_d \tag{21}$$

However,  $HG(s)\theta_d$  cannot be obtained directly. Therefore, the rearrangement of Equation (18) is derived,

$$G(s)u(s) = \frac{\theta_m}{H_0} \tag{22}$$

Therefore,

$$\frac{d\beta}{dt} = -\sigma \frac{H}{H_0} \theta_m \dot{e} = -\acute{\sigma} \theta_m \dot{e} \tag{23}$$

where  $\acute{\sigma} = \sigma \frac{H}{H_0}$ . Thus,

$$\frac{d\beta}{dt} = -\acute{\sigma} \theta_m \dot{e} \tag{24}$$

Equation (24) represents the adjustment of controller parameter  $\beta$  over time. By integration of Equation (24) with respect to time  $t$ , we can have

$$\beta = \int_0^t -\acute{\sigma} \theta_m \dot{e} dt + \beta_0 \tag{25}$$

where  $\beta_0 = [K_0 \ \Lambda_0]^T$  are the initial values of controller parameters that can be optimized by the GA and PSO.

### 5. Stability Analysis

The system stability with IMRAC is analyzed via the Lyapunov stability theory.

In Equation (5), let us assume that  $\theta_d$  is constant. Therefore,

$$\dot{e} = -\dot{\theta}; \quad \ddot{e} = -\ddot{\theta} \tag{26}$$

Reconsidering the general dynamic in Equation (1), we have

$$u = -M\ddot{e} - C\dot{e} + G \tag{27}$$

$$\ddot{e} = M^{-1}u + M^{-1}C\dot{e} - M^{-1}G \tag{28}$$

Equation (4) is rewritten as follows

$$Z = D \begin{bmatrix} e \\ \dot{e} \end{bmatrix} M^{-1} \tag{29}$$

where  $D$  is given as follows,

$$D = \begin{bmatrix} \beta I^{4 \times 4} & 0 \\ 0 & I^{4 \times 4} \end{bmatrix} \tag{30}$$

where  $\beta$  is a positive constant matrix and  $I^{4 \times 4}$  is an identity matrix. Equation (29) in a state space is described as follows

$$\dot{S} = D \begin{bmatrix} \dot{e} \\ \ddot{e} \end{bmatrix} \tag{31}$$

$$\dot{Z} = D \begin{bmatrix} \dot{e} \\ M^{-1}u + M^{-1}C\dot{e} - M^{-1}G \end{bmatrix} \tag{32}$$

$$\dot{Z} = D \begin{bmatrix} 0 & I^{4 \times 4} \\ 0 & M^{-1}C \end{bmatrix} \begin{bmatrix} e \\ \dot{e} \end{bmatrix} + D \begin{bmatrix} 0 \\ M^{-1} \end{bmatrix} u \tag{33}$$

$$\dot{Z} = D \begin{bmatrix} 0 & I^{4 \times 4} \\ 0 & M^{-1}C \end{bmatrix} D^{-1}Z + D \begin{bmatrix} 0 \\ M^{-1} - M^{-1}Gu^{-1} \end{bmatrix} u \tag{34}$$

$$\dot{Z} = AZ + Bu \tag{35}$$

where

$$A = D \begin{bmatrix} 0 & I^{4 \times 4} \\ 0 & M^{-1}C \end{bmatrix} D^{-1}, B = D \begin{bmatrix} 0 \\ M^{-1} - M^{-1}Gu^{-1} \end{bmatrix} \tag{36}$$

If a positive definite matrix  $P \in \mathbb{R}^{n \times n}$  exists, the following equation is satisfied,

$$A^T P + PA = -Q \tag{37}$$

where  $Q \in \mathbb{R}^{n \times n}$  is a positive definite symmetric matrix. Then, a positive-definite Lyapunov function candidate is chosen as follows,

$$V = \frac{1}{2} Z^T P Z \tag{38}$$

Integrating Equations (36)–(38) yields

$$\dot{V} = \frac{1}{2} \dot{Z}^T P Z + \frac{1}{2} Z^T P \dot{Z} \tag{39}$$

$$\dot{V} = \frac{1}{2} (Z^T A^T + u^T B^T) + \frac{1}{2} Z^T P (AZ + Bu) \tag{40}$$

$$\dot{V} = \frac{1}{2} (Z^T A^T P Z + u^T B^T P Z + Z^T P A Z + Z^T P B u) \tag{41}$$

$$\dot{V} = -\frac{1}{2} Z^T Q Z + \frac{1}{2} u^T B^T P Z + \frac{1}{2} Z^T P B u \tag{42}$$

Therefore,

$$\dot{V} \leq \frac{1}{2} u^T B^T P Z + \frac{1}{2} Z^T P B u \tag{43}$$

The output of the controller determined is bounded  $|u| \leq \sigma$ , where the  $\sigma$  is a positive constant.  $B$  and  $P$  are assumed to be positive definite matrices.  $Z$  is dependent on the steady-state error  $e$  and its derivative  $\dot{e}$ . By  $t \rightarrow \infty$ ,  $e \rightarrow 0$  and  $\dot{e} < 0$ . Consequently,  $Z < 0$ . Therefore, we have

$$\dot{V} < \frac{1}{2} \tau^T B^T P Z + \frac{1}{2} Z^T P B u < \gamma \tag{44}$$

where  $\gamma$  is a positive constant. It is concluded that  $\dot{V}$  is bounded within a specific range and it is proven that the control system is asymptotically stable [28].

### 6. Results and Discussion

The optimal controller tuned by GA and PSO are validated for the wearable lower-limb rehabilitation exoskeleton. In addition, we compared the optimal tuned controller and Ziegler–Nichols (Z-N) as a conventional method. The unit step response is applied as a reference to the mathematical model of the exoskeleton represented in Equation (2). The tuned controllers are compared with the unit step response as shown in Figure 6. Table 5 represents the average error (AE) and rise time for GA, PSO, and Z-N.

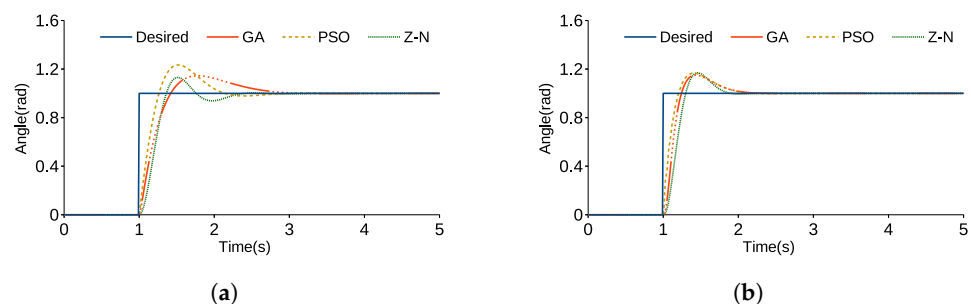


Figure 6. Step response for closed-loop controller system. (a) Hip; and (b) Knee.

**Table 5.** Error and rise time for step response.

Joint	Hip			Knee		
	GA	PSO	Z-N	GA	PSO	Z-N
AE	0.0511	0.0485	0.0585	0.0302	0.03211	0.04448
Rise time	1.2411	1.1967	1.3406	1.1366	1.1500	1.1954

According to Table 5, the AE of PSO for hip is the lowest value by 0.0485 radian and this value of GA for knee has the lowest value by 0.0302 radian. Furthermore, the rise time for the PSO and GA of hip and knee are the lowest among the other method of tuning by 1.1967 and 1.1366 s, respectively. Therefore, the parameters of the PSO and GA are selected as the initial value for IMRAC for the hip and knee, respectively.

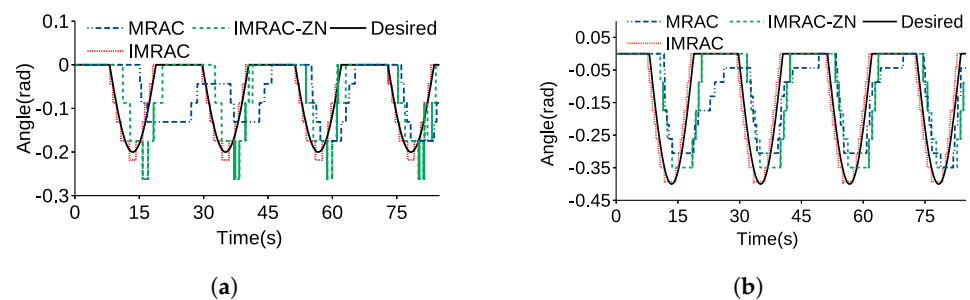
The experiment is conducted on a walking lower-limb rehabilitation robot. One healthy subject (male, 32 years old, height 176 cm, weight 90 kg) is required to wear the robot. He is asked to walk forward for 78 s on the flat ground. Figure 7 represents the snapshots of the subject wearing our wearable lower-limb rehabilitation robot.



**Figure 7.** The walking snapshots of the subject wearing the wearable lower-limb rehabilitation exoskeleton.

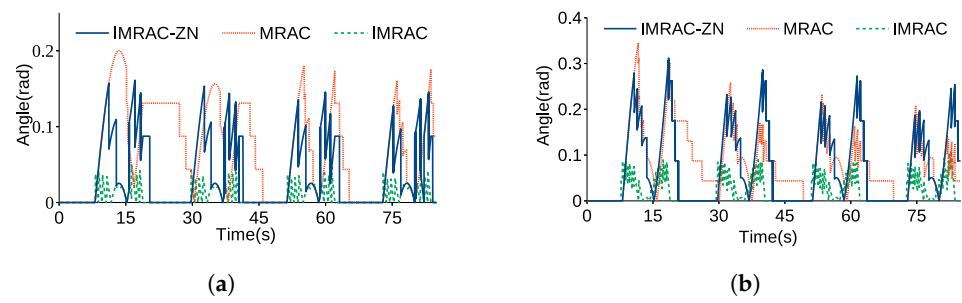
In the experiment, we employed model reference adaptive controller (MRAC), IMRAC, and IMRAC-ZN under the same conditions. This comparison was carried out to observe the effect of initialization for the adaptive controller design. IMRAC-ZN is initialized by Z-N to represent the difference between the optimal and conventional initialization of IMRAC.

Figure 8 compares the angular trajectories of the IMRAC, IMRAC-ZN, and MRAC for the hip and knee, respectively. Since the controller gains of IMRAC and IMRAC-ZN are initialized, they converged more quickly than MRAC.



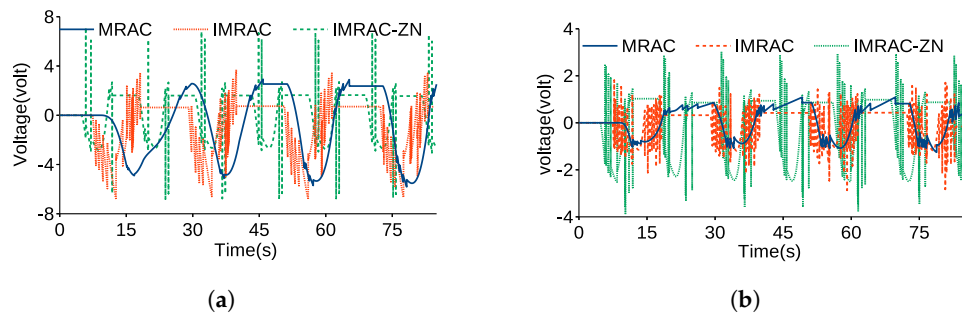
**Figure 8.** Comparison of an angular trajectory for MRAC, IMRAC-ZN, and IMRAC. (a) Hip; (b) Knee.

Figure 9 illustrates the angular trajectory error of IMRAC-ZN, MRAC, and IMRAC for each joint.



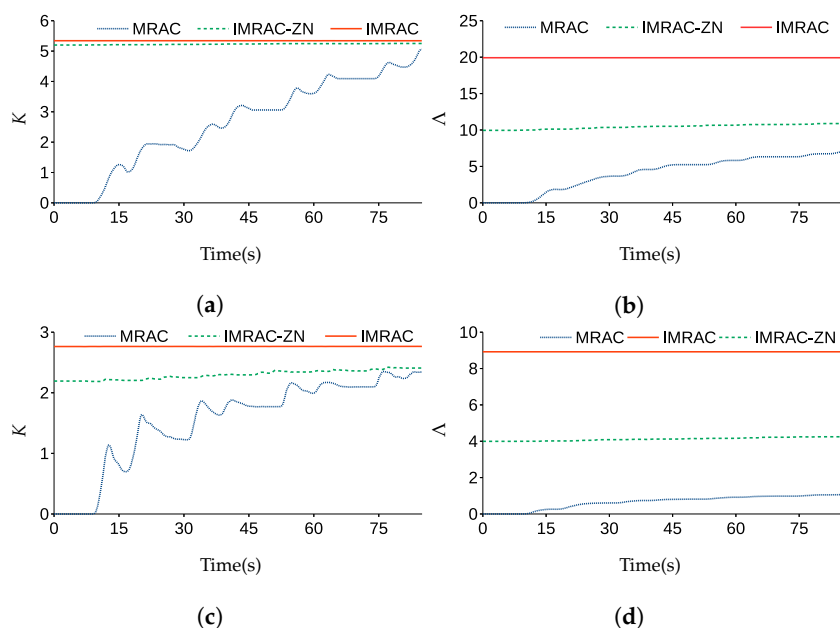
**Figure 9.** Comparison of an angular trajectory error for MRAC, IMRAC-ZN, and IMRAC. (a) hip; and (b) knee.

Figure 10 illustrates the voltage of each joint, which are periodic graphs. The voltage for IMRAC and IMRAC-ZN reacts faster than MRAC since the controller gains are adjusted faster for IMRAC and IMRAC-ZN than MRAC. In addition, the measured voltage of hip is greater than it is for the knee. This is why the actuator of the hip carries the weight of the femur and tibia while the knee actuator only handles the weight of the tibia.



**Figure 10.** Actual voltage of each joint. (a) hip; and (b) knee.

The changes in  $K$  and  $\Lambda$ , for IMRAC, IMRAC-ZN, and MRAC are represented in Figure 11. The initial parameters for MRAC and IMRAC-ZN are set to zero and the controllers are tuned by ZN method, respectively. The controller gains for MRAC, raised from zero, show how the MRAC adjusts the controller gains, while they are constant without considerable changes for IMRAC and IMRAC-ZN, because these are initialized based on GA, PSO, and ZN.



**Figure 11.** Changes in controller gains. (a)  $K$  for hip; (b)  $\Lambda$  for hip; (c)  $K$  for knee; and (d)  $\Lambda$  for knee.

Table 6 exhibits a statistical analysis, i.e., AE, a maximum error (ME) and a root mean square (RMS) of the error of each joint for IMRAC, IMRAC-ZN, and MRAC.

**Table 6.** Statistical analysis comparison.

Joints	Hip			Knee		
	ME	AE	RMS	ME	AE	RMS
MRAC	0.2	0.079	0.0929	0.3450	0.0823	0.1074
IMRAC-ZN	0.1611	0.0375	0.0593	0.3118	0.0724	0.1100
IMRAC	0.0488	0.0079	0.01318	0.1096	0.0199	0.0328

ME of the hip and joint by MRAC is higher than IMRAC and IMRAC-ZN, which concludes the efficiency of IMRAC. However, IMRAC has the lowest error because it is initialized based on the optimization methods for hip and knee. The RMS of IMRAC is the lowest in comparison with the two other methods. For instance, it is 86% and 78% less than MRAC and IMRAC-ZN for the hip.

Based on the experimental results, we concluded that the exoskeleton's trajectory follows the desired trajectory for a periodic walking experiment. Moreover, based on the experimental results, it can be ascertained that the tracking error is bounded within a range. In general, our proposed control system performed efficiently.

## 7. Conclusions

This paper presented a novel IMRAC strategy initialized via optimal controller tuning for wearable lower-limb rehabilitation robots. The tuning of the controller gains is defined as an optimization problem, in which the objective function is the ITAE of steady-state error. Two optimization methods including GA and PSO are established for tuning controller gains optimally. Their performance was compared in the step response of the simulated mathematical model of the wearable lower-limb rehabilitation robot. Furthermore, the IMRAC method is used for controlling the angular trajectory of the wearable lower-limb rehabilitation robot, which is initialized by GA and PSO.

Our proposed IMRAC has been utilized in the lower-limb exoskeleton to assist physiotherapists in rehabilitation training. The exoskeleton prototype used for validation has fixed frames and is specifically designed for average-height subjects. It can be ascertained that the optimal adaptive control strategy can observe the effect of the wearer's forces on its performance for a variety of exercises using a wearable lower-limb rehabilitation exoskeleton.

**Author Contributions:** Conceptualization, M.S.A. and R.R.; methodology, M.S.A., R.R. and A.B.; software, M.S.A.; validation, M.S.A., R.R. and A.B.; formal analysis, M.S.A., R.R. and A.B.; investigation, M.S.A. and R.R.; resources, M.S.A.; data curation, M.S.A. and R.R.; writing—original draft preparation, M.S.A.; writing—review and editing, M.S.A. and R.R.; visualization, M.S.A.; supervision, R.R. and A.B.; project administration, R.R.; funding acquisition, R.R. All authors have read and agreed to the published version of the manuscript.

**Funding:** The authors would like to thank Universiti Kebangsaan Malaysia (UKM) for the financial support received under research grant DIP-2022-005.

**Data Availability Statement:** Not applicable.

**Conflicts of Interest:** The authors declare no conflict of interest.

## References

- Kimura, T.; Horikoshi, Y.; Kuriyagawa, C.; Niiyama, Y. Rho/rock pathway and noncoding rnas: Implications in ischemic stroke and spinal cord injury. *Int. J. Mol. Sci.* **2021**, *22*, 11573. [[CrossRef](#)]
- Lin, P.H.; Dong, Q.; Chew, S.Y. Injectable hydrogels in stroke and spinal cord injury treatment: A review on hydrogel materials, cell-matrix interactions and glial involvement. *Mater. Adv.* **2021**, *2*, 2561–2583. [[CrossRef](#)]
- Hu, S.; Wu, G.; Wu, B.; Du, Z.; Zhang, Y. Rehabilitative training paired with peripheral stimulation promotes motor recovery after ischemic cerebral stroke. *Exp. Neurol.* **2022**, *349*, 113960. [[CrossRef](#)] [[PubMed](#)]

4. Murray, S.A.; Ha, K.H.; Hartigan, C.; Goldfarb, M. An assistive control approach for a lower-limb exoskeleton to facilitate recovery of walking following stroke. *IEEE Trans. Neural Syst. Rehabil. Eng.* **2015**, *23*, 441–449. [[CrossRef](#)] [[PubMed](#)]
5. Chen, B.; Zhong, C.H.; Zhao, X.; Ma, H.; Guan, X.; Li, X.; Liang, F.Y.; Cheng, J.C.Y.; Qin, L.; Law, S.W.; et al. A wearable exoskeleton suit for motion assistance to paralysed patients. *J. Orthop. Transl.* **2017**, *11*, 7–18. [[CrossRef](#)]
6. Kang, Y.; Ding, H.; Zhou, H.; Wei, Z.; Liu, L.; Pan, D.; Feng, S. Epidemiology of worldwide spinal cord injury: A literature review. *J. Neurorestoratology* **2017**, *6*, 1–9. [[CrossRef](#)]
7. Aliman, N.; Ramli, R.; Haris, S.M. Modeling and co-simulation of actuator control for lower limb exoskeleton. In Proceedings of the 2018 3rd International Conference on Control and Robotics Engineering (ICCRE), Nagoya, Japan, 20–23 April 2018; pp. 94–98. [[CrossRef](#)]
8. Merayo, N.; Juárez, D.; Aguado, J.C.; De Miguel, I.; Durán, R.; Fernández, P.; Lorenzo, R.M.; Abril, E. PID Controller Based on a Self-Adaptive Neural Network to Ensure QoS Bandwidth Requirements in Passive Optical Networks. *J. Opt. Commun. Netw.* **2017**, *9*, 433. [[CrossRef](#)]
9. Pan, Z.; Dong, F.; Zhao, J.; Wang, L.; Wang, H.; Feng, Y. Combined Resonant Controller and Two-Degree-of-Freedom PID Controller for PMSLM Current Harmonics Suppression. *IEEE Trans. Ind. Electron.* **2018**, *65*, 7558–7568. [[CrossRef](#)]
10. Huo, W.; Mohammed, S.; Amirat, Y.; Kong, K. Active Impedance Control of a lower limb exoskeleton to assist sit-to-stand movement. In Proceedings of the IEEE International Conference on Robotics and Automation, Stockholm, Sweden, 16–21 May 2016; pp. 3530–3536. [[CrossRef](#)]
11. Lin, J.; Divekar, N.V.; Thomas, G.C.; Gregg, R.D. Optimally Biomimetic Passivity-Based Control of a Lower-Limb Exoskeleton over the Primary Activities of Daily Life. *IEEE Open J. Control Syst.* **2022**, *1*, 15–28. [[CrossRef](#)]
12. Lu, R.; Li, Z.; Su, C.Y.; Xue, A. Development and learning control of a human limb with a rehabilitation exoskeleton. *IEEE Trans. Ind. Electron.* **2014**, *61*, 3776–3785. [[CrossRef](#)]
13. Tu, Y.; Zhu, A.; Song, J.; Shen, H.; Shen, Z.; Zhang, X.; Cao, G. An adaptive sliding mode variable admittance control method for lower limb rehabilitation exoskeleton robot. *Appl. Sci.* **2020**, *10*, 2536. [[CrossRef](#)]
14. Huang, P.; Li, Z.; Zhou, M.; Li, X.; Cheng, M. Fuzzy Enhanced Adaptive Admittance Control of a Wearable Walking Exoskeleton with Step Trajectory Shaping. *IEEE Trans. Fuzzy Syst.* **2022**, *30*, 1541–1552. [[CrossRef](#)]
15. Shan, H.; Jiang, C.; Mao, Y.; Wang, X. Design and control of a wearable active knee orthosis for walking assistance. In Proceedings of the IEEE 14th International Workshop on Advanced Motion Control, AMC, Auckland, New Zealand, 22–24 April 2016; pp. 51–56. [[CrossRef](#)]
16. Belkadi, A.; Oulhadj, H.; Touati, Y.; Khan, S.A.; Daachi, B. On the robust PID adaptive controller for exoskeletons: A particle swarm optimization based approach. *Appl. Soft Comput.* **2017**, *60*, 87–100. [[CrossRef](#)]
17. Zhang, Q.; Zhang, X.; Yin, G.; Yang, K.; Xie, J.; Han, X. Design on subsection based mix position controller for lower limb rehabilitation robot. In Proceedings of the 14th International Conference on Ubiquitous Robots and Ambient Intelligence, URAI, Jeju, Republic of Korea, 28 June–1 July 2017; pp. 720–724. [[CrossRef](#)]
18. Yang, Y.; Huang, D.; Dong, X. Enhanced neural network control of lower limb rehabilitation exoskeleton by add-on repetitive learning. *Neurocomputing* **2019**, *323*, 256–264. [[CrossRef](#)]
19. Amiri, M.S.; Ramli, R.; Ibrahim, M.F. Genetically optimized parameter estimation of mathematical model for multi-joints hip–knee exoskeleton. *Robot. Auton. Syst.* **2020**, *125*, 103425. [[CrossRef](#)]
20. Amiri, M.S.; Ramli, R.; Tarmizi, M.A.A.; Ibrahim, M.F.; Danesh Narooei, K. Simulation and Control of a Six Degree of Freedom Lower Limb Exoskeleton. *J. Kejuruter.* **2020**, *32*, 197–204. [[CrossRef](#)] [[PubMed](#)]
21. Amiri, M.S.; Ramli, R.; Ibrahim, M.F.; Wahab, D.A.; Aliman, N. Adaptive Particle Swarm Optimization of PID Gain Tuning for Lower-Limb Human Exoskeleton in Virtual Environment. *Mathematics* **2020**, *8*, 2040. [[CrossRef](#)]
22. Mirjalili, S.; Song, J.; Lewis, D. *Nature-Inspired Optimizers*; Springer: Berlin/Heidelberg, Germany, 2020.
23. Zhang, Y.; Wang, S.; Ji, G. A Comprehensive Survey on Particle Swarm Optimization Algorithm and Its Applications. *Math. Probl. Eng.* **2015**, *2015*, 931256. [[CrossRef](#)]
24. Abdmouleh, Z.; Gastli, A.; Ben-brahim, L.; Haouari, M. Review of optimization techniques applied for the integration of distributed generation from renewable energy sources. *Renew. Energy* **2017**, *113*, 266–280. [[CrossRef](#)]
25. Amiri, M.S.; Ramli, R.; Aliman, N. Adaptive Swarm Fuzzy Logic Controller of Multi-Joint Lower Limb Assistive Robot. *Machines* **2022**, *10*, 425. [[CrossRef](#)]
26. Gerasimov, D.N.; Ortega, R.; Nikiforov, V.O. Relaxing the high-frequency gain sign assumption in direct model reference adaptive control. *Eur. J. Control* **2018**, *43*, 12–19. [[CrossRef](#)]
27. Najafi, A.; Spencer, B.F. Adaptive model reference control method for real-time hybrid simulation. *Mech. Syst. Signal Process.* **2019**, *132*, 183–193. [[CrossRef](#)]
28. Amiri, M.S.; Ramli, R. Utilisation of Initialised Observation Scheme for Multi-Joint Robotic Arm in Lyapunov-Based Adaptive Control Strategy. *Mathematics* **2022**, *10*, 3126. [[CrossRef](#)]

**Disclaimer/Publisher’s Note:** The statements, opinions and data contained in all publications are solely those of the individual author(s) and contributor(s) and not of MDPI and/or the editor(s). MDPI and/or the editor(s) disclaim responsibility for any injury to people or property resulting from any ideas, methods, instructions or products referred to in the content.